This is a “preproof” accepted article for *Mineralogical Magazine*.

This version may be subject to change during the production process.

10.1180/mgm.2024.101

Mechanisms and factors influencing the removal/recovery of gold nanoparticles by thermally modified pyrite

Yuhong Fu[*a], Shanshan Zhang[a], Qin Liu [a], Shanshan Li[b], Shuai Zhang [a], Sen Li[a], Can Wu[a], Meimei Ran[a]

a. School of Geography and Environmental Sciences, Guizhou Normal University, Guiyang 550025, China

b. School of Chemistry and Materials Science, Guizhou Normal University, Guiyang 550025, China

*Corresponding author:

Name: Yuhong Fu

Email: fuyuhong24@163. com

Mailing address: Comprehensive Science Laboratory Building. Guizhou Normal University. Guiyang 550025, China

Manuscript Submission Date: 2024. 7. 18

Abstract

The environmental effects of nanoparticles have attracted widespread attention. The removal and recycling of nanoparticles are crucial for both environmental protection and resource reuse. However, current removal and recycling methods are not yet mature, and there is a need to explore inexpensive materials for the efficient removal and recycling of nanoparticles. This study investigates the effects of pyrite species, thermal modification temperature, pH, and ionic strength on the adsorption of gold nanoparticles (AuNPs) by pyrite. The experimental results demonstrate that the adsorption rate of artificially thermally modified pyrite is slightly faster than that of naturally thermally modified pyrite. However, the concentration of Fe ions dissolved from the artificially thermally modified pyrite is higher. Natural pyrite, when thermally modified at 400°C and 500°C, adsorbs 100% of AuNPs within 10 minutes. The lower the acidity of the system, the

faster the adsorption rate. Conversely, an increase in ionic strength decreases the adsorption rate. Artificially thermally modified pyrite primarily adsorbs AuNPs through electrostatic gravitational attraction, which is supplemented by a significant amount of chemisorption. After four recycling cycles, the adsorption and desorption rates of AuNPs using artificially thermally modified pyrite were 92. 1% and 94. 2%. Respectively, indicating excellent adsorption and recovery performance. The results of this study provide a new method for the recycling of nanoparticles and an experimental basis for the further application of thermally modified pyrite in environmental treatments.

Keywords: Nanoparticles; Pyrite; Thermal modification; Adsorption; Electrostatic attraction.

1, Introduction

Due to their particular physical and chemical properties, engineered nanoparticles (ENPs) are widely used in industry, scientific research, medicine, pharmaceuticals, and everyday items(Lee et al., 2010). Their average annual production is estimated to reach 1 million tonnes(Arturo et al., 2014). Nanoparticles may enter the environment at any stage of their life cycle, such as production, transport, through use and emissions(Keller et al., 2013; Rex et al., 2023). Numerous studies have confirmed the widespread presence of nanoparticles in soil, water, atmosphere, rocks, organisms, and celestial bodies(Banfield et al., 2001; Hochella, 2002; Hochella et al., 2008).

Nanoparticles in the environment can exhibit significant biotoxicity under certain conditions. For instance, studies have demonstrated that gold nanoparticles (AuNPs) possess a higher toxicity potential compared to ionic gold, causing alterations in zebrafish DNA(Dedeh et al., 2015). They also induce inflammation and damage in lung tissue, kidney haemorrhage, liver lymphocyte infiltration, and neuronal damage in mice and rats(Isoda et al., 2020). Under specific conditions, gold nanoparticles can enter the human body. For example through the digestive and dermal systems, directly harming the body by reducing the activity and viability of various cells, including germ cells, dermal fibroblasts, and lung cells(Wiwanitkit et al., 2009; Pernodet et al., 2006; Pan et al., 2007). Furthermore, the impact of nanoparticles (or sols) on the distribution of the major and trace elements they carry and their environmental effects should not be ignored(Novikov et al., 2006). Given the ecological, environmental and economic significance of nanoparticles, there is an urgent need for an efficient and inexpensive adsorbent to recover or remove nanoparticles from waste. Despite the critical importance of nanoparticle recovery and reuse, methods remain immature, and related studies are limited(Kalaitzidou et al., 2023).

Recovery of gold nanoparticles by adsorption using activated carbon fibres in a batch reactor and a microreactor, respectively has been reported by Luty-Błocho et al. (Luty-Błocho et al., 2021), and Krishnamurthy et al. (Krishnamurthy et al., 2021) employed cetyltrimethylammonium bromide, sodium dodecyl sulphate, and sodium citrate (CTAB) to recover gold nanoparticles from biomass. Further, Lazim et al. (Lazim et al., 2010) recovered gold nanoparticles based on the pH-induced heterogeneous aggregation of positive/negative mixed hydrogels. However, these methods are currently costly, and their adsorption efficiency needs further improvement, so they are not very suitable for practical applications.

Pyrite, the most abundant metal sulfide on the earth's surface, is commonly found in various precious metal-associated ores and is, therefore, frequently present in industrial slag and mine tailings. Due to its rich active functional groups and unique physicochemical properties, such as precipitation adsorption and redox(Murphy et al., 2009). Pyrite has attracted extensive attention recently and has been applied in removing pollutants, including heavy metal ions, non-metal ions, and organic pollutants(He et al., 2019; Guo et al., 2020; Rashid et al., 2018). This study uses pure-phase pyrite synthesised through calcination and oxidation thermal modification of natural pyrite and hydrothermal synthesis at different temperatures as an adsorbent for gold nanoparticles. It investigates the effects of thermal modification temperature, pyrite source, pH, and ionic strength. The study also explores methods for the desorption and recovery of adsorbed gold nanoparticles.

2, Materials and Instruments

Natural pyrite from the Liangshuijing mine in Meitan County, Zunyi City, Guizhou Province, was sourced from the bottom of the Wujiaping Formation a stratified layer clay rocks. It was ground to 240–325 mesh (61–45 μm) prior to experimentation. For the expassociated with eriments chloroauric acid trihydrate ($HAuCl_4 \cdot 3H_2O$, ≥99.9%) and carbon disulfide (CS_2, analytically pure) were procured from Aladdin Reagent Company. Additionally, sodium citrate dihydrate ($C_6H_5Na_3O_7 \cdot 2H_2O$, excellent pure), sodium hydroxide (NaOH, analytically pure), nitric acid (HNO_3, 65–68w/%, analytically pure), hydrochloric acid (HCl, 36–38 w/%, analytically pure), and anhydrous ethanol (C_2H_5OH, analytically pure) were acquired from Chongqing Chuandong Chemical Company. Ferrous chloride ($FeCl_2 \cdot 4H_2O$, 99.7%, analytically pure), sodium thiosulfate pentahydrate ($Na_2S_2O_3 \cdot 5H_2O$, 99%, analytically pure), and thiourea (H_2NCSNH_2, analytically pure) were purchased from Chengdu Jinshan Chemical Reagent Co. The gold standard solution (100 μg mL^{-1}) and iron standard solution (1000 μg mL^{-1}) were obtained from the National

Nonferrous Metals Research Institute. All experimental water was pure water.

An open-type horizontal vacuum tube atmosphere furnace (SK-GO6123K, Tianjin Zhonghuan Furnace Corp., China) was utilised to calcinate the adsorbent. A thermostatic oscillator (THC-98AB, Shanghai Yiheng Technology Instrument Co., Ltd., China) was employed for the thermostatic oscillation of the samples to ensure complete contact between the gold nanoparticles and minerals during the adsorption process. The concentrations of Au and Fe were determined using an atomic absorption spectrophotometer (AAS, GGX-800, Beijing Haiguang Instrument Co., Ltd., China). Sample morphology was analysed using a dual-beam scanning electron microscope (SEM, Scios, Hillsboro, OR, USA), and surface characteristic elements and morphology were examined using an energy spectrometer (EDS, FEI Company, USA). The adsorbent's surface potential at room temperature was measured using a multi-angle particle size analyser and a high-sensitivity zeta potential meter (Omni, Brookhaven Instruments, New York, NY, USA) alongside a UV-Vis spectrometer (Cary 300, Agilent Technologies, USA). An X-ray photoelectron energy spectrometer (XPS, K-alpha, Thermo Fisher Scientific K-Alpha, USA) was utilised to measure the component levels and ratios of the samples. Functional groups and crystal structures of the adsorbents were investigated using Fourier Transform Infrared Spectroscopy (FTIR, VERTEX 70, BRUKER OPTICS, Germany) and X-ray Diffraction (XRD, Empyrean, Eindhoven, The Netherlands) mapping.

3, Preparation methods

3. 1 Preparation of gold nanoparticles

The Frens method was utilised to synthesise gold nanoparticles (AuNPs)(Frens, 1973). The synthesis involved the following steps: 600 mL of $HAuCl_4$ solution (0. 01% w/w) was added to a three-necked flask, which was then heated in an oil bath and stirred using a magnetic stirrer. While maintaining the condensation reflux, 25.64 mL of sodium citrate solution (1% w/w) was added to the boiling $HAuCl_4$ solution. The mixture was heated for an additional 20 min before the flask was removed from the oil bath, cooled to room temperature, and stored in a refrigerator at 4°C. The resulting gold nanosolutes were wine-red in colour. Afterwards the mixture was heated for 20 min, then the three-necked flask was again removed from the oil bath and cooled to room temperature before being stored in a refrigerator at 4°C. The prepared gold nanosolid was a burgundy-coloured colloid. A multi-angle particle size analyser (Omni, Brookhaven Instruments, New York, NY, USA) and a UV-Vis spectrometer (Cary 300, Agilent Technologies, USA) were utilised to detect

the particle size and UV-Vis absorption spectra of the AuNPs.

3. 2 Pre-treatment of natural pyrite

Fresh pyrite oxidises easily in air, and an oxidised layer may form on the surface of the mineral within minutes or even seconds(Lu et al., 2005). Therefore, it is essential to pre-treat natural pyrite samples with acid washing before conducting thermal modification experiments or adsorption experiments to obtain fresh, unoxidised pyrite. The natural pyrite was acid-washed and soaked for over 6 h using HCl at a concentration of 3 M to ensure the complete removal of the oxidised layer from the surface of the natural pyrite. Subsequently, it was ultrasonically cleaned with anhydrous ethanol four to five times until the anhydrous ethanol appeared transparent. Following these steps, the samples were placed in a vacuum-drying oven to dry, resulting in fresh pyrite, designated as N-Py.

3. 3 Artificial preparation of pyrite

Artificial pyrite was synthesised using the hydrothermal method as described in the literature(Kaur et al., 2016) to compare the difference in the adsorption properties of natural pyrite and artificial pyrite without impurities after calcination. The procedure involved dissolving 2 g of $FeCl_2 \cdot 4H_2O$ and 8 g of $Na_2S_2O_3 \cdot 5H_2O$ in 80 mL of pure water. The solution was then transferred to an autoclave lined with polytetrafluoroethylene and heated at 200°C in a vacuum oven. Upon cooling the autoclave completely, the black solid was removed, washed with carbon disulfide, and then rinsed with a large amount of deionised water and anhydrous ethanol. The washed pyrite was placed in a vacuum-drying oven and heated for 12 h at 60°C, producing synthetic pyrite labelled S-Py.

3. 4 Natural/artificial pyrite thermal modification methods and characterisation

Fresh natural or artificial pyrite was heated at 100–800°C in a high-purity air atmosphere using an open-type horizontal vacuum tubular atmosphere furnace (SK-GO6123K, Tianjin Zhonghuan Furnace Corp. China), following the procedures described in our previous work(Fu et al., 2024). In genera, air was introduced into the furnace for half an hour before calcination (flow rate: 0.5 L min^{-1}) and continued throughout the heating process (flow rate: 0.25 L min^{-1}). The

heating duration was 2 h. Upon heating, air continued to pass through for an additional hour to allow the furnace to cool to room temperature. The heat-treated pyrite was then transferred from the quartz boat to a drying dish for appropriate preservation. The resulting samples were numbered according to the temperature of thermal modification, with thermally modified natural pyrite and artificial pyrite designated as N-Py-100–N-Py-800 and S-Py-100–S-Py-800, respectively. The morphology and crystal structures of the samples before and after calcination was characterised using an SEM (Scios, Hillsboro, OR, USA) and XRD (Empyrean, Eindhoven, The Netherlands). The surface potential of thermally modified natural pyrite at 500°C (i. e., N-Py-500) was determined using a multi-angle particle size analyser and a high-sensitivity zeta potential meter (Omni, Brookhaven Instruments, New York, NY, USA). The method involved adjusting the initial pH of purified water to 2–11, adding N-Py-500 powder (solid–liquid ratio of 0. 25 g: 50 mL), shaking the well, and then extracting 3 mL for zeta potential measurement. The average value was taken as the measurement result after three repeated measurements.

4, Adsorption experimental methods

The mixtures were placed in an air-bath thermostatic shaker and shaken at 150 rpm and 25°C. They were then subjected to solid–liquid centrifugal separation (100 g, 10 min), followed by the removal of 1 mL of natural/artificial pyrite. Solid–liquid centrifugation (100 g, 10 min) was performed after timed sampling, followed by the removal of 1 mL of supernatant into a 10 mL volumetric flask, and 1 mL of fresh aqua regia was added to each sample for overnight digestion. The concentration of adsorbed remaining Au and mineral-dissolved Fe ions in the supernatant was measured by an AAS (GGX-800, Beijing Haiguang Instrument Co., Ltd., China) after volume adjustment on the second day. Following the adsorption reaction, the solids, labelled N-Py-AuNPs and N-Py-500-AuNPs, respectively, were filtered out, briefly rinsed twice with deionised water of the same pH, placed in a vacuum oven at a set temperature of 60°C, and treated for 6 h before undergoing XRD testing. The surface morphology of the N-Py-AuNPs and N-Py-500-AuNPs samples was observed using a dual-beam SEM (Scios, Hillsboro, OR, USA). The elemental contents of the surfaces were analysed by an energy spectrometer (EDS, FEI Company, USA). The chemical bonding changes in the N-Py-500 samples and the N-Py-500-AuNPs samples were analysed using a Fourier transform infrared spectrometer (FTIR, VERTEX 70, BRUKER OPTICS, Germany). Chemical state changes of Au4f, S2p, Fe2p, and full spectra of N-Py-500 samples and N-Py-500-AuNPs samples were analysed using an XPS (K-alpha, Thermo Fisher Scientific K-Alpha, USA).

4. 1 Effect of pH

Based on the above experimental results, 500℃ thermally modified natural pyrite (i. e., N-Py-500) was selected as the primary research object. The initial pH of the AuNPs sol was adjusted by a small amount of HCl solution or NaOH solution, and the N-Py-500 powder was added to the AuNPs solution with a concentration of ~60 mg/L according to the solid–liquid ratio of 0.25 g : 50 mL. All samples were placed in a thermostatic oscillator at 150 rpm, 25℃, sampled according to the set time, centrifuged (100 g, 10 min), and 1 mL of the supernatant was removed in a 10 mL volumetric flask, 1 mL of fresh aqua regia was added to each sample for overnight elimination, and after the second day of calibration, the concentrations of Au and Fe in the supernatant were measured using AAS. The surface potential of N-Py-500 at different pH was detected using a high-sensitivity zeta potential meter (Omni, Brookhaven Instruments, New York, NY, USA) to further investigate the mechanism of pH effect on the adsorption process.

4. 2 Effect of different ISs.

The ionic strength of AuNPs solutes was adjusted using a small amount of NaCl solution (0.5, 1 and 5 mM NaCl) at 25℃, pH 5.6 and a solid–liquid ratio of 0. 25 g:50 mL to understand the effect of ionic strength on the adsorption system. Moreover, adsorption experiments were performed by adding 0.25 g of N-Py-500 powder to 50 mL of AuNPs solution (the sampling and measurement procedure was kept the same as above). After the adsorption experiments, the concentration changes of Au and Fe were tested using AAS.

4. 3 Removal of Fe ions

In the adsorption experiments, some Fe ions were found to be dissolved, requiring extra controls to be put in place, in order to prevent secondary pollution. The experimental method was as follows: at the end of the reaction between N-Py-500 and AuNPs sol, 5 g of $Ca(OH)_2$ solid (concentration of 1.35 mol/L after addition) was added to precipitate Fe ions. Samples were collected at set time points by drawing 5 mL of the mixture with a 5 mL pipette and placing it in centrifugal tubes, which were centrifugated at 150 rpm and 25℃. The samples were drawn at a fixed time point by taking 1 mL of the supernatant in a 10 mL volumetric flask, which was shaken at 150 rpm. Solid–liquid centrifugation (100 g, 10 min) was performed after timed sampling, followed by collection of 1 mL of supernatant in a 10 mL volumetric flask. Thereafter, 1 mL of fresh aqua regia was added to each sample for overnight elimination. Finally, the changes in the concentration of Fe ions and Au in the samples were tested on the second day using AAS.

4. 4 AuNPs desorption and adsorbent reusability study

In order to study the recovery of gold and the reusability of N-Py-500, the adsorption-desorption experiments were carried out using water (repeated once) and a mixture of 10% thiourea and 2% HCl (repeated four times) as desorption agents respectively. Firstly, the adsorption experiment was carried out as before: the pH was adjusted to 5. 6, the solid–liquid ratio of was 0. 25 g : 50 mL, and AuNPs concentration was 60 mg/L. N-Py-500 was added and oscillated for adsorption at room temperature for 4 h. After completion of the adsorption, the solid samples were taken out and dried in a vacuum-drying oven (60℃, 3 h). The desorption experiments were also performed according to the solid–liquid ratio of 0. 25 g : 50 mL, and the adsorbed Au-containing N-Py-500-AuNPs and desorbent were subjected to constant temperature oscillation at room temperature for 4 h. After sampling according to the set time points, the samples were centrifuged and separated, and the supernatant was tested for the concentration of desorbed Au and the concentration of dissolved Fe ions by AAS. The desorbed minerals were rinsed with purified water 4 to 5 times and then dried in a vacuum-drying oven (60°C, 3 h), and the dried minerals were again reacted with AuNPs (pH 5.6, concentration 60 mg/L) according to the solid–liquid ratio (0.25 g : 50 mL) for the adsorption experiments at room temperature, and this adsorption–desorption was repeated four times (when used a mixture of 10% thiourea and 2% HCl as desorption agents).

4. 5 Calculation of adsorption/desorption rates

The concentration of AuNPs in the adsorption system where adsorption did not occur was measured using AAS, from which the adsorption amount and adsorption rate of AuNPs on minerals were calculated. The desorption amount and desorption rate were determined from the concentration of AuNPs in the supernatant after desorption. The calculation process is as follows:

$$Q_t = \frac{(C_0 - C_t) * V}{\mathrm{m}_1} \quad (1)$$

$$\mathrm{W} = \frac{C_0 - C_t}{C_0} \times 100\% \quad (2)$$

$$Q_e = \frac{C_1 * V_1}{m_2} \quad (3)$$

$$\eta = \frac{Q_e}{Q_t} \times 100\% \quad (4)$$

Where Q_t is the adsorption amount of AuNPs by minerals at time t. C_0 is the initial concentration of AuNPs in the adsorption system. C_t is the concentration of AuNPs in the adsorption system where adsorption does not occur. V is the volume of AuNPs, Where m_1 is the

mass of pyrite. W is the adsorption rate. Q_e is the amount of desorption. C_1 is the concentration of AuNPs in the supernatant of the desorbed solution. V_1 is the volume of the solution when desorbed. Where m_2 is the mass of pyrite being desorbed. Where η is the desorption rate.

5, Results and discussion

5. 1 Characterisation of materials

5. 1. 1 Gold nanoparticles

In this study, burgundy colloids of AuNPs were synthesised using the Frens method. The synthesised AuNPs were characterised using an ultraviolet-visible spectrophotometer (UV-Vis) and a multi-angle particle size analyser, along with a highly sensitive zeta potential meter. The UV-Vis detection, as illustrated in Fig. 1, indicated that the absorbance peak of AuNPs was at 519 nm with a notably narrow half-peak width, consistent with the spectral characteristics of well-dispersed gold sols. Table 1 shows the average particle size of 19.06 nm and a polydispersity coefficient of 0.166, measured after repeating the test three times on the synthesised AuNPs sol by Dynamic Light Scattering. This indicated a relatively uniform particle size distribution. The zeta potential of AuNPs was detected as −29.87 mV using the multi-angle particle size analyser and the high-sensitivity zeta potential meter.

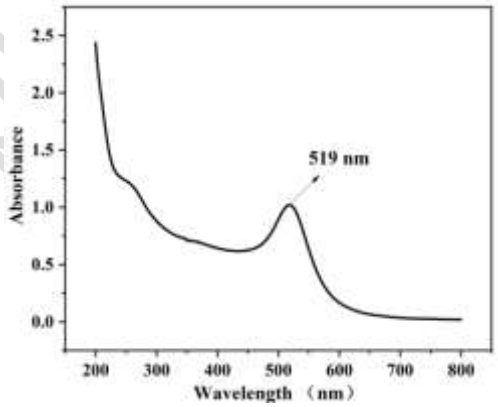

Figure 1 UV-Vis absorbance spectrum of AuNPs

Table 1 Particle size and Zeta potential of AuNPs

Serial Number	Grain Size (nm)	Polydispersity Factor	Zeta Potential (mV)
1	19.11	0.154	−27.56
2	19.10	0.174	−30.68

3	18.97	0.169	−31.38
Average Value	19.06	0. 166	−29.87

5. 1. 2 Pyrite

The XRD patterns of natural and artificial pyrite before and after thermal modification were characterized in our previous study (Fu et al., 2024). N-Py and S-Py align closely with the PDF card (JCPDS card no. 71-2291) of pyrite, indicating their high purity. The XRD peaks of N-Py-100–300 and S-Py-100–300 occupy approximately the same positions with the main peak of pyrite, which is probably due to the relatively low content of oxidised pyrite resulting from the low temperature of the thermal modification. Thus, no other minerals were detected. The highest peak occurs at the (121) crystal face of N-Py-400, which exhibits the best crystallinity. It has been noted that a thermal modification temperature of 400°C significantly enhances the magnetic recovery of pyrite to 80%(Waters et al., 2008), potentially contributing to the superior adsorption effect of N-Py-400 in the adsorption experiments with AuNPs (refer to 5. 2. 1 for details). S-Py-400 corresponds to the standard PDF card of magnetite (JCPDS card no. 88-0315), indicating a phase transformation to magnetite. N-Py-500–800 and S-Py-500–800 which develop new crystalline facets such as (110), (024), (231), and (130), correlate with hematite (JCPDS card no. 72-0469), marking a transformation in the main composition of the sample from pyrite to hematite after calcination above 500°C(Li. 2016).

The morphology of N-Py, before and after thermal modification, was analysed using a double-beam SEM (Fig. 2). The surface of N-Py exhibited fine pits, probably due to acid corrosion during pre-treatment (Fig. 2-a). Figures 2b to 2e illustrate that the mineral particle size remained relatively constant after thermal modification. However, spherical particulate matter emerged on the surface of all samples, increasing in quantity as the thermal modification temperature rose. The spherical particulate matter was distributed uniformly across the surface of the minerals in N-Py-400 (Fig. 2-e). Figure 2f shows the topography of N-Py-500, which also displays numerous spherical particles on the surface and a more pronounced layer structure. The morphology of S-Py samples before and after thermal modification is shown in Fig. 3. S-Py is characterised by smaller size and aggregation, resembling strawberry pyrite with small particles (Fig. 3a). The overall morphology of S-Py-100 to S-Py-300 resembles that of S-Py (Fig. 3b to 3d). The edges of S-Py-400 and S-Py-500 particles transition from sharp to smooth (Fig. 3e to 3f), and there is a notable increase in both the number of spherical materials on the surface and the particle size compared to other (S-Py-100 to 300) minerals.

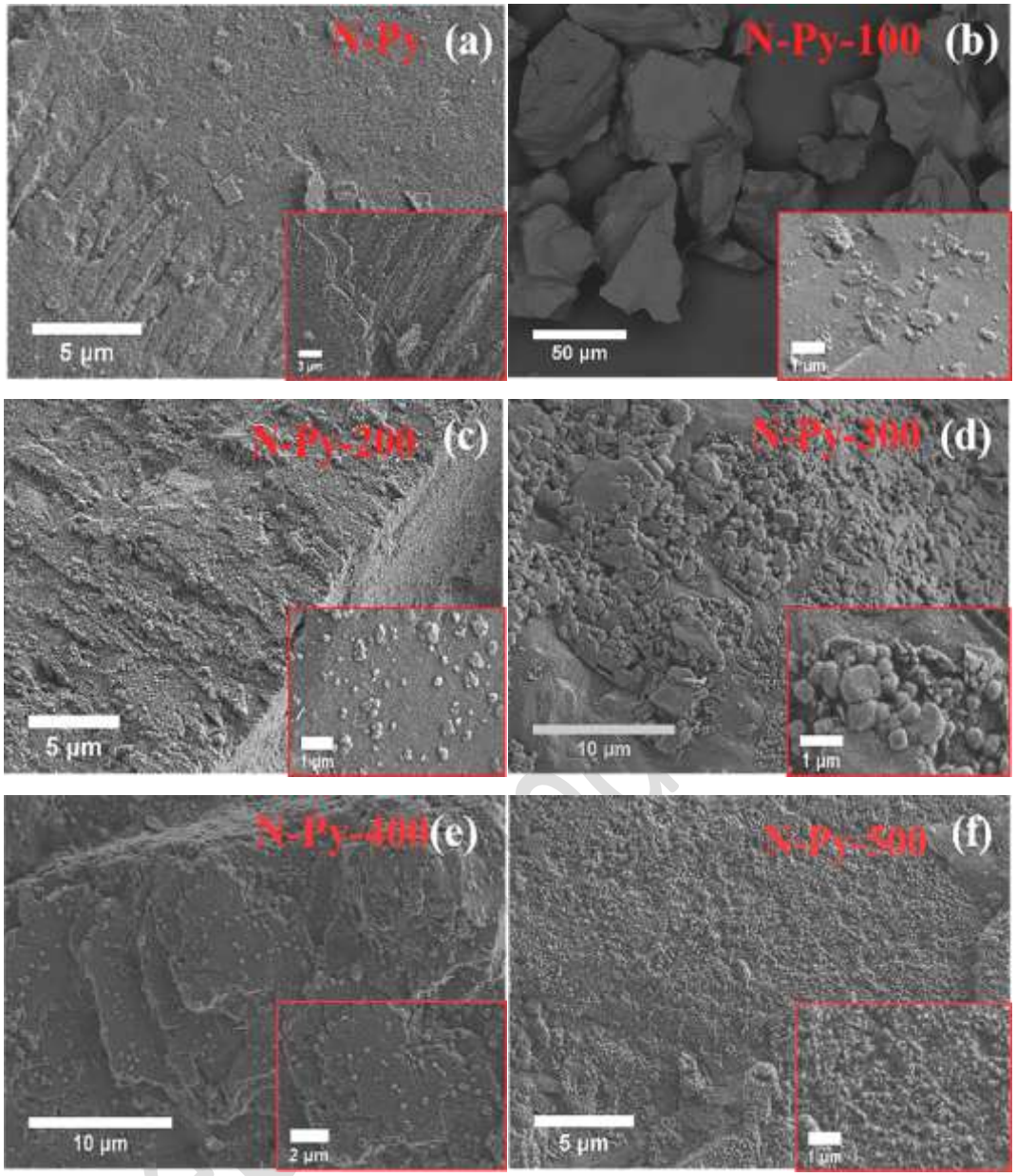

Figure 2. SEM images of N-Py (a) and N-Py-100–500 (b–f).

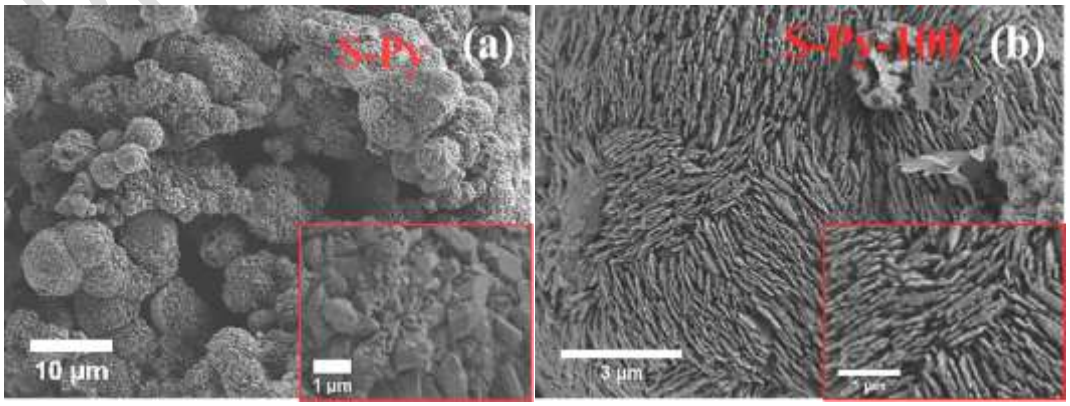

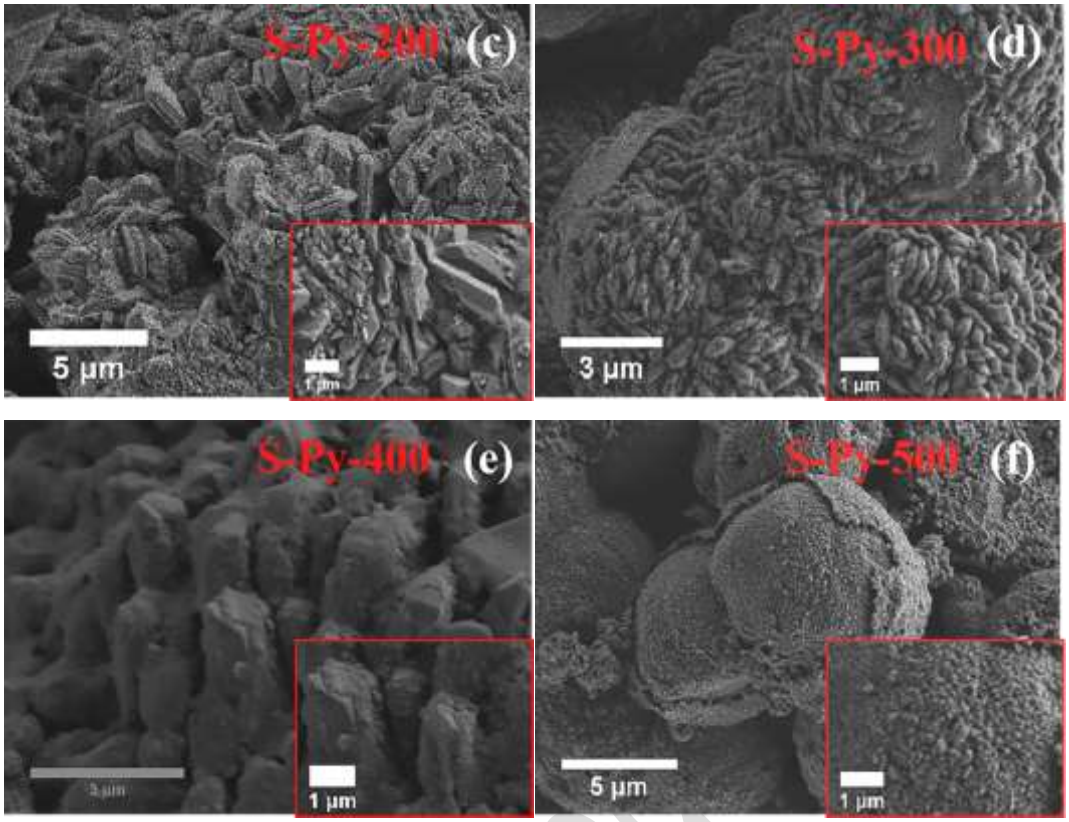

Figure 3. SEM images of S-Py (a) and S-Py-100–500(b–f).

5. 2 Pyrite after thermally modified oxidation

5. 2. 1 Effect of thermal modification temperatures

In order to compare the effects of different thermal modification temperatures and pyrite sources on the adsorption of AuNPs, experiments were conducted using natural/artificial pyrite with various thermal modification temperatures at a reaction temperature of 25°C, pH 5.6, and a solid–liquid ratio of 0.25 g:50 mL. Figure 4a shows the adsorption of AuNPs by N-Py before and after thermal modification. N-Py-400 demonstrated the fastest adsorption rate, completing the process almost instantaneously, followed by N-Py-500, which completed adsorption within 10 minutes. For N-Py-100, 200, and 300, the concentration of AuNPs decreased gradually; however, adsorption equilibrium was not reached even after 72 hours. Conversely, N-Py-600, 700, 800, and N-Py adsorbed AuNPs at the same rate and exhibited minimal adsorption.

From the analysis of Fe concentration variations (Fig. 4b), N-Py-400 exhibited the highest level of Fe ion dissolution, approximately 160 mg L^{-1}. The Fe ion dissolution concentrations in the N-Py-100, 200, 300, and 500 systems at 72 h ranged between 43 and 57 mg L^{-1}. In contrast,

the Fe ion dissolution concentrations in the N-Py-600 and N-Py systems were 12 and 15 mg/L at 72 h, respectively. The lowest Fe ion dissolution occurred in N-Py-700 and 800, where the concentrations were only 2.132 and 1.904 mg L^{-1} at 72 h. Pyrite calcined at 400°C and 500°C had the highest adsorption capacity for Au. This can be attributed to the fact that some of the FeS_2 was converted to Fe_2O_3 under medium-temperature calcination. The two were mixed together with stronger physicochemical properties, more adsorption sites, and a larger specific surface area, resulting in the fastest adsorption efficiency. As the calcination temperature increases, the vast majority of FeS_2 is converted to Fe_2O_3, and the decrease in physicochemical properties can lead to a reduction in adsorption efficiency(He et al., 2019).

The adsorption duration was extended in Fig. 4c to explore the adsorption capacity of N-Py on AuNPs. The concentration of AuNPs showed negligible reduction during the initial 8 days. However, a rapid decrease occurred from the 8th day onward. By the 14th day, the AuNPs concentration in the adsorption system had reached 0 mg L^{-1}, indicating an adsorption efficiency of 100%. Over time, the amount of solubilised Fe ions increased, reaching 88.331 mg L^{-1} by the 17th day. The solid XRD plots of N-Py and N-Py-AuNPs (adsorbed for 17 days) (Fig. 4d) revealed sharp peaks at 2θ values of 25.867, 38.748 and 57.695, which were identified as metallic Au peaks(Fan et al., 2014). Given that the isoelectric point (pH_{IEP}) of unoxidised pyrite is typically around 2 (Luo et al., 2018), N-Py remains negatively charged in the absence of oxidation and does not adsorb negatively charged AuNPs due to electrostatic repulsion in the study system. Nevertheless, as reaction time increased, partial oxidation of N-Py and a probable decrease in the stability of AuNPs in the adsorption system led to reduced AuNPs concentrations from the 8th day onward, attributed to self-agglomeration and adsorption (see section 5. 2. 6 Mechanistic analysis for details).

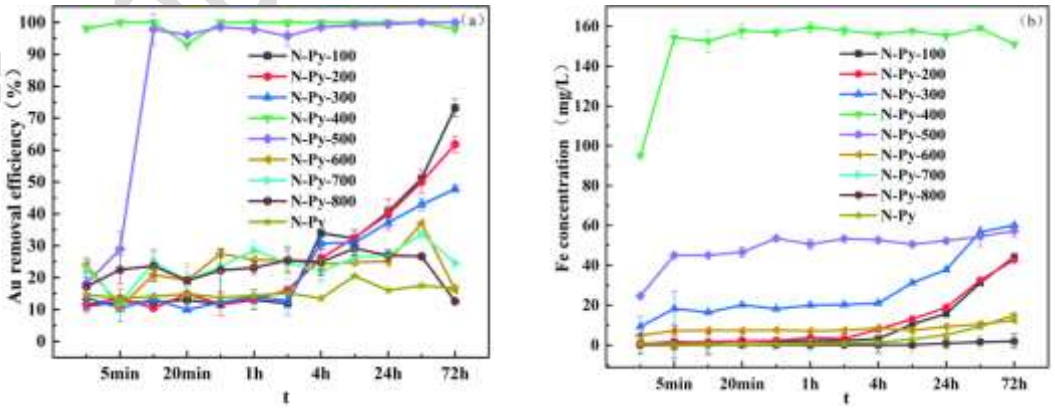

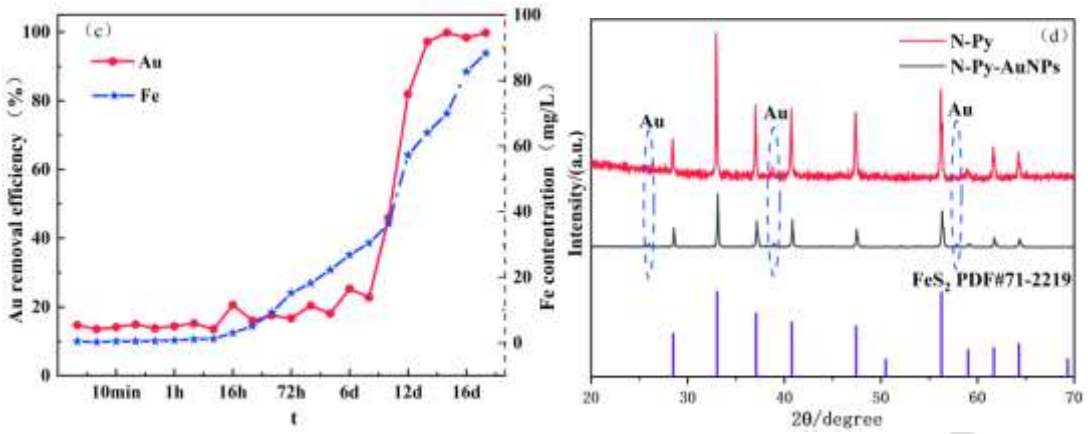

Figure 4. Changes in Au removal efficiency (a) and Fe concentration (b) in the adsorption of AuNPs by N-Py before and after thermal modification; Au adsorption efficiency and Fe concentration in the adsorption of AuNPs by N-Py (c); XRD image of AuNPs adsorbed by N-Py (d).

In experiments on AuNPs adsorption by S-Py at various thermal modification temperatures (Fig. 5a). S-Py-300 demonstrated the most effective adsorption, achieving an adsorption efficiency of 87.7% (remaining AuNP concentration of 6.996 mg L^{-1}) at the 0 min sampling mark. S-Py-400 followed, completing most of its adsorption by 5 min, with an adsorption efficiency of 91.5% (remaining AuNP concentration of 4.818 mg L^{-1}). S-Py-500 completely adsorbed the gold nanoparticles within 10 min. S-Py-200 showed limited adsorption of AuNPs for up to 4 h, but a significant increase in adsorption began at 16 h. The adsorption efficiency reached 48% at 16 h, and most adsorption was concluded by 24 h, reaching an efficiency of 95.8%. The adsorption efficiencies of S-Py and S-Py-100 were comparable, with nearly complete adsorption occurring by 72 h.

From the analysis of Fe ion dissolution (Fig. 5b), compared to the thermally modified N-Py system, the overall Fe ion dissolution in the thermally modified S-Py system was higher during the adsorption process. The Fe ion dissolution of S-Py-400 reached 539.9 mg L^{-1} at 5 min and then remained at equilibrium. The subsequent highest Fe ion dissolution was observed in S-Py-500 at 5 min, where it recorded 328.8 mg L^{-1} of Fe ions, after that fluctuating around 300 mg L^{-1}. S-Py, S-Py-100, S-Py-200, S-Py-300, S-Py-600, and S-Py-700 exhibited the largest Fe ion dissolution. The quantity of Fe ions dissolved by these samples increased linearly from 4 h; however, the dissolution by S-Py-300 was higher and occurred more rapidly. No Fe ion dissolution was observed during the adsorption of S-Py-800.

Comparing the adsorption capacities of thermally modified N-Py and S-Py at the same temperature, the latter showed a stronger overall adsorption capacity. For instance, at a thermally modified temperature of 300°C, N-Py-300 did not complete the adsorption of AuNPs within 72 h, whereas S-Py-300 completed the process within seconds. This difference could be attributed to the

fact that the particle size of thermally modified S-Py is only about one-fourth that of N-Py, and its surface is rougher, with many grooves and more adsorption sites. When comparing the adsorption behaviours of N-Py and S-Py, N-Py barely adsorbed AuNPs over 8 days, while S-Py fully adsorbed AuNPs within 72 h. This difference is probably due to the ease with which pyrite oxidises in aqueous solutions, producing oxidation products on the mineral surfaces(Luo et al., 2018); the oxidation process is more rapid for S-Py due to its much smaller particle size.

In summary, although the adsorption rate of thermally modified S-Py is relatively quick, the benefit is not markedly significant. In contrast, the Fe ion dissolution is noticeably higher. Meanwhile, thermally modified N-Py remains an adsorbent with good economic efficiency and effective adsorption capability. Among the thermally modified N-Py samples, N-Py-400 adsorbed AuNPs at the fastest rate. Nevertheless, the amount of Fe ions dissolved was almost three times that of other temperatures, leading to the selection of N-Py-500, which had the second-best effect in adsorbing AuNPs for subsequent adsorption reactions.

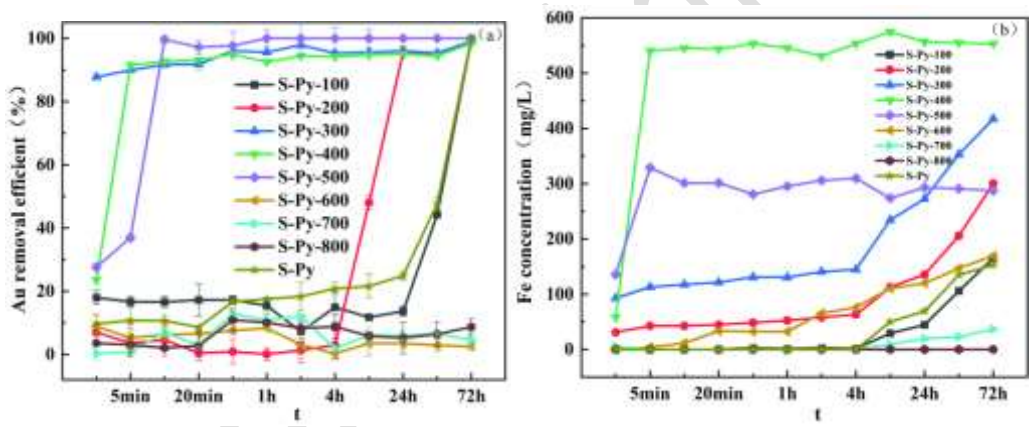

Figure 5 Changes in Au removal efficiency (a) and Fe concentration (b) in the adsorption of AuNPs by S-Py before and after thermal modification

5. 2. 2 Effect of pH on adsorption

In order to investigate the effect of the initial pH of the solution on the adsorption of AuNPs by N-Py-500, the initial pH range was set at 2, 3, 4, 5, 6, 7, 8, 9, and 10 at room temperature. The adsorption reaction was conducted using 0.25 g of N-Py-500 with 50 mL of AuNPs sol. The experimental results are shown in Fig. 6a. The lower the initial pH, the faster the rate of AuNPs adsorption. In the adsorption system with an initial pH of 2, AuNPs were adsorbed in 0 min. This was followed by the adsorption systems with initial pH of 3, 4, 5 and 6, where AuNPs were adsorbed by N-Py-500 in 30 min. In the system with an initial pH of 7, the adsorption of AuNPs was significantly slowed, completing in 6 h. Under alkaline conditions, the concentration of AuNPs was only slightly reduced in the adsorption systems with initial pH of 8, 9, and 10. From

the adsorption rate at 6 h of reaction (Fig. 6b), the adsorption efficiency of N-Py-500 for AuNPs remained almost constant at more than 98% in the range of initial pH 2–7. Starting from an initial pH of 8, the adsorption efficiency gradually decreased as the solution pH increased, with the adsorption efficiency being only ~20% at pH 10. The change in solution pH leads to a change in surface charge between N-Py-500 and AuNPs. To further investigate the effect of pH on the adsorption process, the isoelectric point (pH_{IEP}) of N-Py-500 was determined to be 10.1 (Fig. 7). In the acidic system, the adsorption of AuNPs was favoured due to the electrostatic attraction between the positively charged N-Py-500 and the negatively charged AuNPs. With the gradual increase in pH, the positive charge on the surface of N-Py-500 was reduced, and the electrostatic attraction to AuNPs decreased. When the pH exceeded the pH_{IEP}, electrostatic repulsion between AuNPs and N-Py-500 occurred, preventing adsorption.

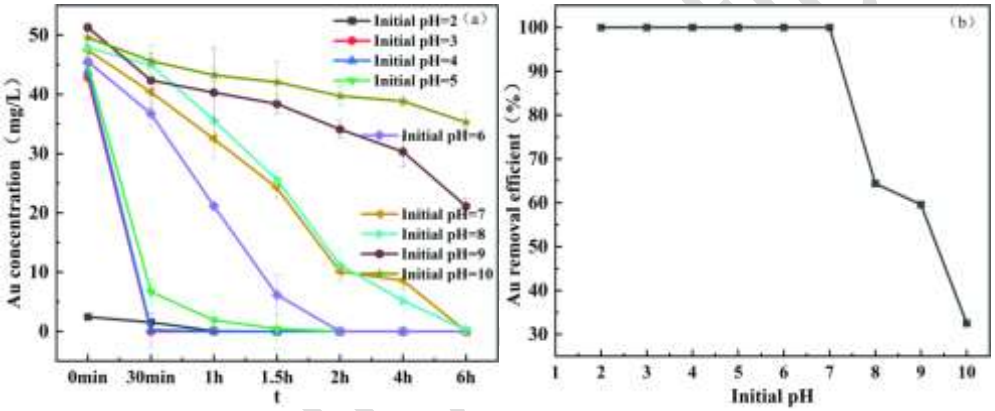

Figure 6. The residual AuNPs (a) and removal efficiency of AuNPs (b) in the adsorption of AuNPs by N-Py-500 as a function of initial pH.

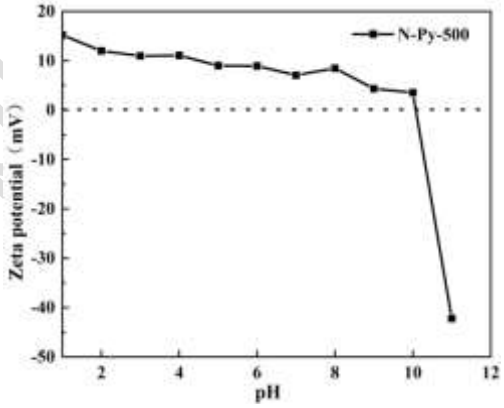

Figure 7. Zeta potential image of N-Py-500.

From the Fe ion dissolution (Fig. 8a), the amount of Fe ions dissolved was essentially the same in acidic and basic adsorption systems with no significant difference. The concentration of Fe dissolved at 6 h ranged from 92.574 to 105.245 mg L^{-1}. It appears that Fe ions do not change due to the pH variation of the adsorption system, which also indicates that the N-Py-500 sample is relatively stable. After some of the unstable Fe ions on the surface of the sample dissolved, no

further dissolution of Fe ions occurred. The change in pH during the adsorption experiment is shown in Fig. 8b. Except for the adsorption system with an initial pH of ~2, the pH of all other adsorption systems decreased, eventually becoming acidic.

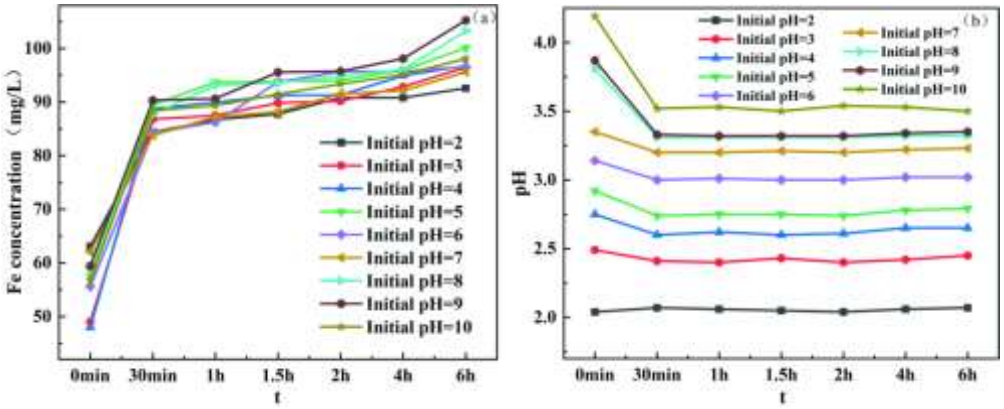

Figure 8. Dissolution of Fe ions (a) and the changes in pH (b) during the adsorption of AuNPs by N-Py-500 as a function of initial pH.

5. 2. 3 Effect of ionic strength on adsorption

Ionic strength ranges of 0.05, 1 and 5 mM NaCl were set at room temperature (25°C), and the adsorption reaction was performed using 0.25 g of N-Py-500 with 50 mL of AuNPs sol. The Au concentration in the blank control group, which did not contain minerals and only adjusted the ionic strength of the AuNPs sol, did not change significantly. The fluctuations were within the error range, indicating that the ionic strength range set in the experiment would not affect the stability of the AuNPs sol itself (Fig. 9a). The effect of ionic strength on the adsorption of AuNPs by N-Py-500 is shown in Fig. 9b. Comparing adsorption samples with unadjusted and adjusted ionic strength, the adsorption samples without adjusted ionic strength and the adsorbed samples with unadjusted ionic strength are shown in Fig. 9b. The fastest rate of adsorption of AuNPs was observed when ionic strength was adjusted. The rate of decrease in AuNPs concentration was significantly reduced in the adsorption systems with ionic strength of 0.05 mM and 1 mM NaCl. This reduction might be caused by ionic strength compressing the double electric layer of N-Py-500 and AuNPs and inhibiting the electrostatic attraction between them. Furthermore, with an increase in ionic strength, the adsorption rate in the ionic strength 5 mM NaCl adsorption system increased again, which may be due to the decrease in repulsion between the AuNPs adsorbed on N-Py-500 and those approaching from the suspension, thereby favouring an increase in the adsorption rate to some extent(Jiang et al., 2021).

As shown in Fig. 9c. Ionic strength did not have much effect on the dissolution of Fe ions, which consistently remained around 90 mg L^{-1} regardless of the ionic strength level. Additionally,

the addition of ionic strength appeared to inhibit the decrease of pH in the adsorption system (Fig. 9d). The pH of the adsorption system with ionic strength of 0.05, 1 and 5 mM NaCl eventually stabilised at ~3, while the adsorption system without ionic strength addition decreased to around 2-7.

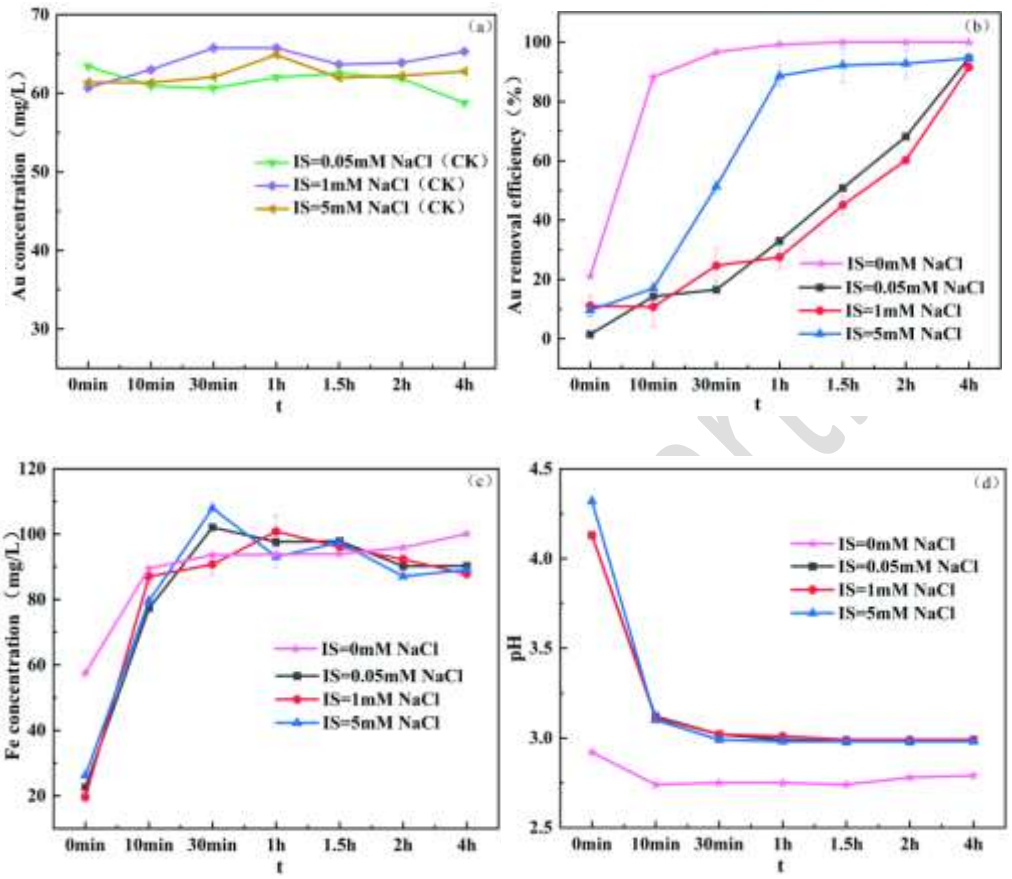

Figure 9. (a) Changes in Au concentration of blank control samples; (b) removal efficiency of AuNPs; (c) Fe ions dissolution; (d) pH changes in the adsorption of AuNPs by N-Py-500 as a function of ISs.

5. 2. 4 Removal of Fe ions

Although N-Py-500 adsorbed AuNPs effectively, the adsorption process was accompanied by a certain amount of Fe ion leaching under various experimental conditions (different pH and ionic strength). Therefore, to control the amount of Fe ions dissolved during the adsorption of AuNPs by N-Py-500, an excess of alkali was added to convert Fe ions into $Fe(OH)_2$ or $Fe(OH)_3$ and precipitate them, which achieved the removal of AuNPs ions without introducing a new source of contamination (Fe ions) and simultaneously neutralised the excess acid. Fe ion removal experiments were performed using experimental samples at different ionic strength (temperature of 25°C, pH of 5.6, solid–liquid ratio of 0.25 g:50 mL, AuNPs concentration of approximately 60

mg L^{-1}, and ionic strengths of 0.05, 1, and 5 mM NaCl). Additionally, 5 g of $Ca(OH)_2$ (with a concentration of 1.35 mol L^{-1}) was added to the vials of the sample that had completed the adsorption, as shown in Fig. 10. The Fe concentration decreased almost instantly. Moreover, no Fe ions were detected at 0 min, proving that the addition of excess $Ca(OH)_2$ can solve the problem of Fe ion dissolution quickly (Fig. 10a). Moreover, although the addition of a large amount of $Ca(OH)_2$ caused the adsorption system to shift from acidic to alkaline, it did not significantly affect the adsorbed AuNPs, with no phenomena such as desorption or agglomeration of AuNPs observed (Fig. 10b). This indicates that the addition of $Ca(OH)_2$ effectively reduced the release of Fe without impacting the adsorption performance of the adsorbent on AuNPs.

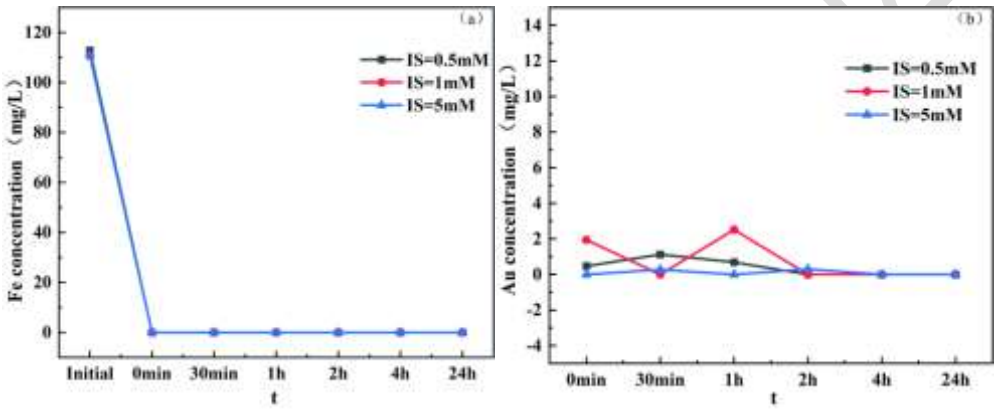

Figure 10 Changes in Fe concentration (a) and Au concentration (b) after the addition of $Ca(OH)_2$.

5. 2. 5 Desorption experiments and adsorbent reusability studies

In order to further explore the reusability of AuNPs and investigate whether N-Py-500 is reusable, N-Py-500, which had previously adsorbed AuNPs, was desorbed before repeating the adsorption and desorption experiments. Initially, pure water with a pH adjusted to 5.6 served as the desorption agent, and the results are presented in Fig. 11a. Even after 18 days of desorption, the quantity of AuNPs desorbed was minimal, with only 2–3 mg L^{-1} of AuNPs being successfully desorbed.

A reagent mixture of 10% thiourea and 2% hydrochloric acid was selected as the desorbent (Fig. 11a). The first desorption rate reached only 53.2%, and after desorption, a second round of adsorption was conducted, with the adsorption rate still at 97.1%. Subsequently, four adsorption-desorption experiments were carried out, and the adsorption efficiency decreased from 100% to 92.1%, while the desorption efficiency increased from 53.2% to 94.2%. The repeated desorption experiments indicated that increased desorption frequency improved desorption

efficiency. This improvement is likely due to the destabilisation of AuNPs on the N-Py-500 surface under the repeated action of the desorbent mixture of 10% thiourea and 2% hydrochloric acid, leading to higher desorption efficiency. Since AuNPs were not fully desorbed in each cycle, repeated adsorption-desorption experiments resulted in more adsorption sites on the N-Py-500 surface being occupied by AuNPs, thus decreasing the adsorption capacity. However, the adsorption rate remained at 92.1%, demonstrating the good reusability of N-Py-500.

Figure 11b shows that no Fe ions were dissolved within 4 hours when pure water was used as the desorbent during the adsorption–desorption experiments. However, when the 10% thiourea and 2% hydrochloric acid mixture were used, Fe ion dissolution occurred. Within 4 hours, the amount of Fe ions dissolved in the first desorption experiment was 35 mg L^{-1}, and in the second to fourth desorption experiments, the amounts were 63.8, 48.38, and 26.74 mg L^{-1}, respectively. During the adsorption experiments, the amount of Fe ions dissolved in the first adsorption process was larger, at 95. 52 mg L^{-1}, but subsequently, the amount dissolved was almost negligible.

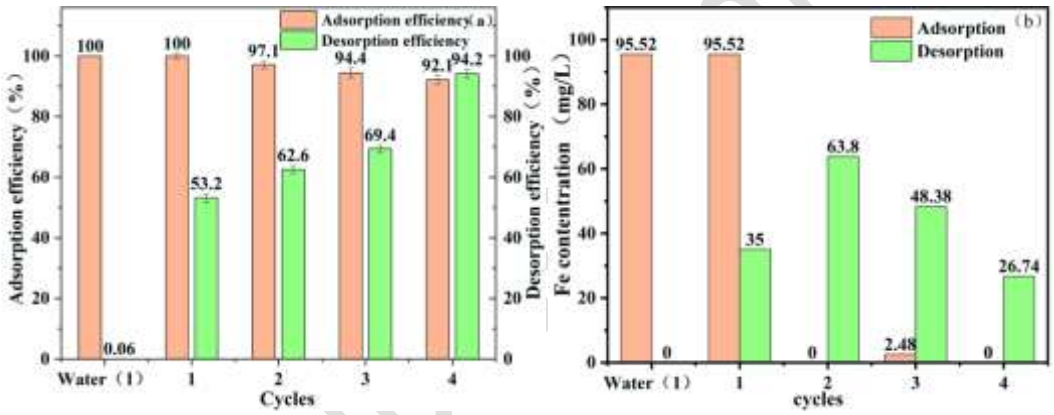

Figure 11. (a) Adsorption-desorption behavior of AuNPs on N-Py-500 surface; (b) dissolution of Fe in adsorption-desorption experiments.

5. 2. 6 Adsorption mechanism

SEM-EDS analyses of N-Py-500 and N-Py samples (designated N-Py-500-AuNPs and N-Py-AuNPs, respectively) after adsorption of AuNPs are shown in Figs 12–14. The Au peaks were clearly observed in EDS for both samples, alongside the peaks of Fe and S. A certain amount of uniformly dispersed nanoscale white dots appeared in the SEM backscattering images of N-Py-500-AuNPs (Fig. 12, Fig. 14a), indicating uniform adsorption of AuNPs on the N-Py-500 surface. In contrast, a large number of white agglomerates appeared on the mineral surface of N-Py-AuNPs (Fig. 13, Fig. 14b). Pyrite hardly adsorbs AuNPs due to electrostatic repulsion when it is not oxidized(Jiang et al., 2021), and the adsorption time of N-Py-AuNPs in this assay was 17 days. The extended adsorption period led to the agglomeration of AuNPs in the system and the oxidation of N-Py, resulting in the precipitation and adsorption of AuNPs agglomerates on the

mineral surface.

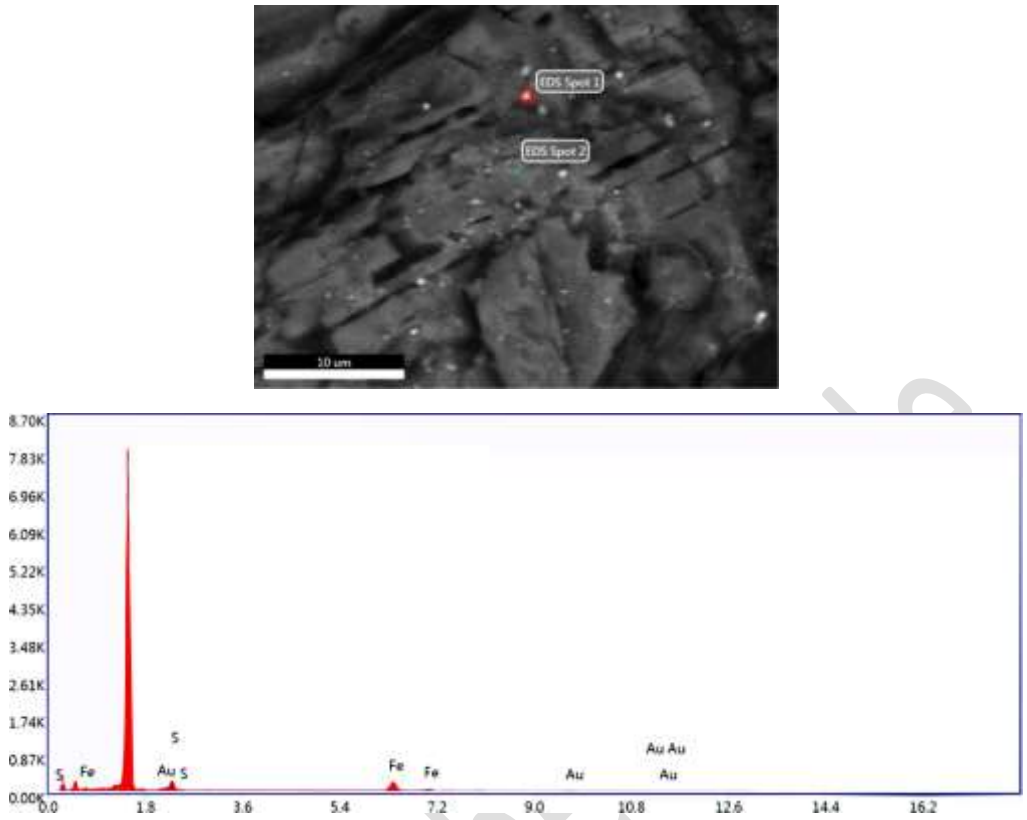

Figure 12. SEM-EDS image of N-Py-500-AuNPs.

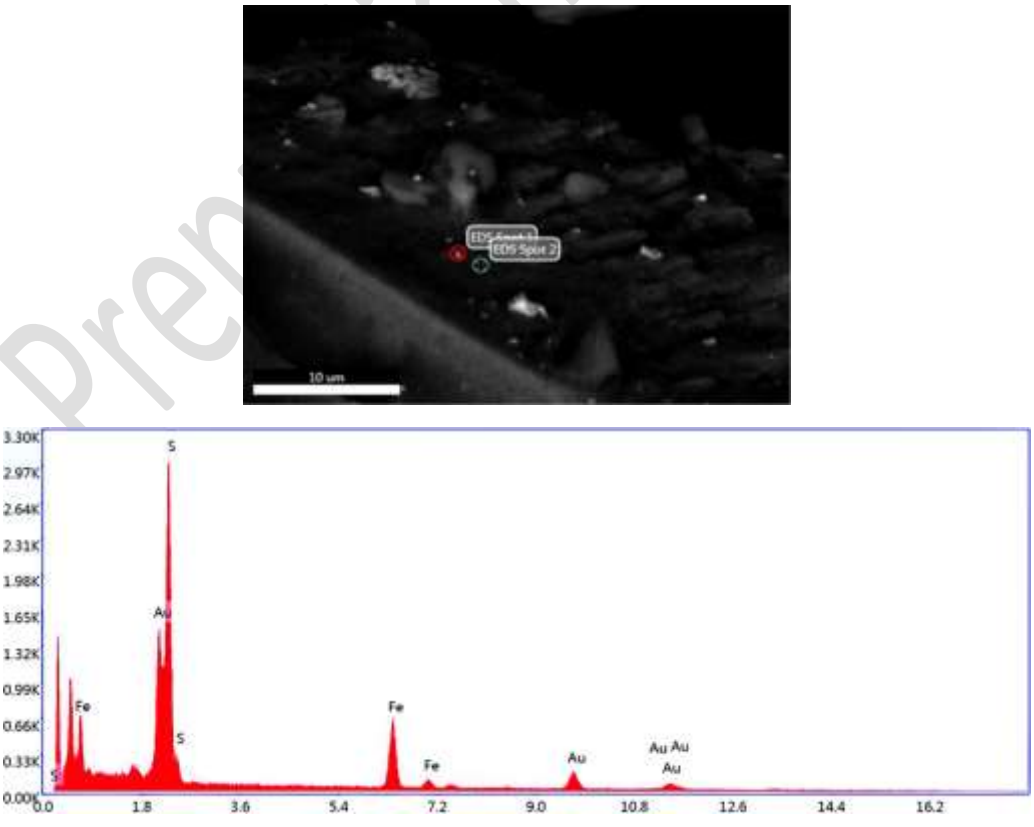

Figure 13. SEM-EDS image of N-Py-AuNPs.

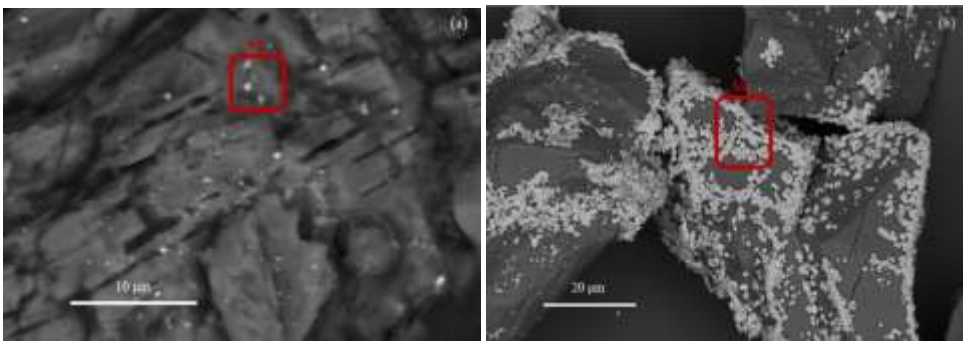

Figure 14. SEM images: (a) N-Py-500-AuNPs; (b) N-Py-AuNPs.

The FTIR spectra of N-Py-500 before and after adsorption of AuNPs are shown in Fig. 15. The peak value of SO_4^{2-} was 1127.3 cm^{-1} before adsorption, and the peak value was obviously weakened after adsorption, indicating that the SO_4^{2-} content on the surface of N-Py-500-AuNPs might be reduced(Kenzhaliyev et al., 2023)**Error! Reference source not found.**. The Fe–O bond was 482.8 cm^{-1} before adsorption, and it shifted to 480.4 cm^{-1} after adsorption, suggesting that the Fe-O bond might play an important role in the N-Py-500 adsorption of AuNPs, indicating that the Fe-O bond may play an important role in the adsorption of AuNPs by N-Py-500 (Dong et al., 2022).

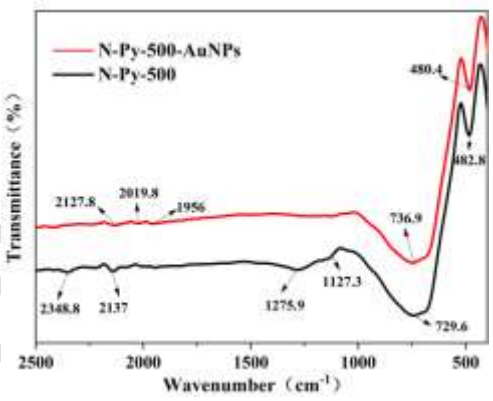

Figure 15. FTIR spectra of samples of N-Py-500 and N-Py-500-AuNPs.

Samples of N-Py-500 and N-Py-500-AuNPs were subjected to XPS analysis (Fig. 16) to further analyse the adsorption mechanism. The appearance of the Au 4f peak in the full XPS spectrum (Fig. 16a) further proves that the AuNPs have been successfully attached to N-Py-500. Comparing the Fe2p spectra of N-Py-500 and N-Py-500-AuNPs (Fig. 16b), the binding energy of Fe^{3+}-O changed from 710.18 to 709.97 eV; the binding energy of Fe^{3+} changed from 713.8 to 712.83 eV, 718.07 to 718.65 eV, and 731.38 to 732.8 eV, while the binding energy of Fe^{2+} changed from 723.65 to 723.23 eV and from 724.88 to 724.54 eV, respectively. Combined with the shifting of the Fe–O bond in the FTIR analyses, these results suggest that certain chemical changes occur before and after the adsorption of AuNPs by N-Py-500. Therefore, in addition to

the electrostatic adsorption effect between N-Py-500 and AuNPs sol, the Fe–O functional group may also bind to the gold in the sol through chelation.

In Fig. 16c, when comparing the S2p spectra of N-Py-500 and N-Py-500-AuNPs, the binding energies of SO_4^{2-} changed from 169.12 and 169.77 eV to 168.3 and 169.53 eV, respectively. Whereas there was the presence of S_2^{2-} belonging to pyrrhotite (163.29 eV) in N-Py-500(Yang et al., 2021), the N-Py-500-AuNPs did not show S_2^{2-}, which suggests that the sulfur-containing functional groups of N-Py-500 may be involved in the adsorption process and oxidised. When analysed in conjunction with the XPS results, the S can be attributed mainly to the conversion from S_2^{2-} to n-hexavalent SO_2^{4-}, which produces complex intermediates that need to be proved by further analytical studies(Jiang et al., 2021).

The Au 4f peaks can be divided into Au 4f7/2 and Au 4f5/2 (Fig. 16d), which involve different gold chemical states, including Au^0 (83.91 eV, 87.59 eV), and Au^{1+} (82.29 eV) (Yang et al., 2021). The sols of AuNPs prepared by reducing chloroaurate with citrate were analysed using XPS by previous authors, and it was found that they contained Au^{1+} (Mikhlin et al., 2009; Park et al., 2014), but their binding energies were located at approximately 85–88 eV, which was quite different from the binding energy position of Au^{1+} in the N-Py-500-AuNPs mapping. Therefore, the Au^{1+} in N-Py-500-AuNPs likely originated from chelation and other chemical reaction processes.

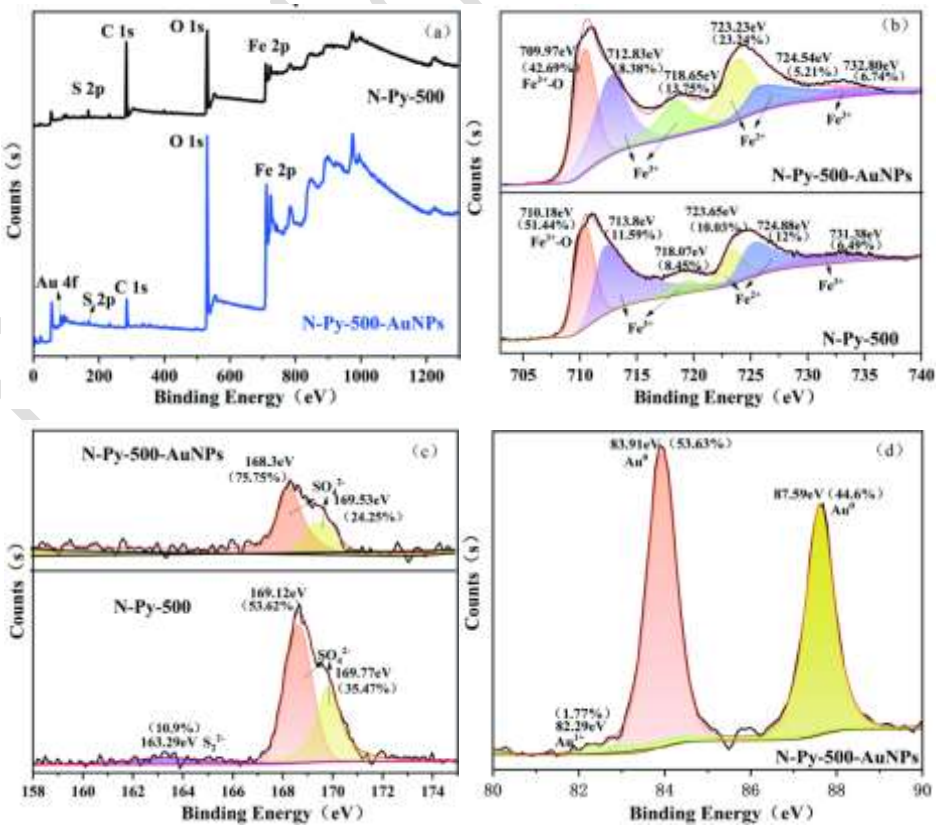

Figure 16 XPS spectra of N-Py-500 and N-Py-500-AuNPs, (a) full spectrum; (b) Fe 2p; (c) S 2p; (d) Au 4f

Combined with the analysis of the effects of pH and ionic strength on the adsorption process (see Sections 5. 2. 2 and 5. 2. 3), electrostatic attraction is the main mechanism for the adsorption of AuNPs by N-Py-500. In addition, Fe-O functional groups and sulfur-containing functional groups in N-Py-500 may be involved in the adsorption process through chelation or electron transfer, potentially leading to the generation of Au(I). It is noteworthy that, in contrast to N-Py-500, which required only 10 min for the complete adsorption of AuNPs, a previous study found that pure hematite required 6 days for the complete adsorption of gold nanoparticles under similar experimental conditions (Wang et al., 2023) N-Py-500, composed of hematite/pyrite, showed significantly better adsorption capacity than hematite. This finding is consistent with previous studies that found the product of the transformation process from Fe(II) to Fe(III) hydrogen/oxide has a higher adsorption capacity than the direct utilisation of Fe(III)(He et al., 2019; Amstaetter et al., 2010).

6, Conclusions

The release of gold nanoparticles from various products can pose a risk to the ecosystem, hence this investigation has explored using low-cost materials that can efficiently capture gold nanoparticles and effectively remove them from the environment. Natural and artificial pyrite was thermally modified at different temperatures (100–800°C) and its ability to remove/recover gold nanoparticles investigated. Factors such as thermal modification temperature, pyrite purity, adsorption time, pH, and ionic strength were examined in relation to the adsorption effect. In addition, possible secondary contamination caused by the leaching of Fe ions during the adsorption process was successfully controlled. It was found that natural pyrite (N-Py-500) calcined at 500°C can effectively adsorb AuNPs within 10 min (at pH 5.6).

The Fe ion leaching was within a controllable range, and the cost was relatively low. Due to electrostatic attraction, the higher the acidity of the system, the faster the adsorption of N-Py-500 with AuNPs. The increase in the ionic strength, as compared to the unapplied ionic strength, can be attributed to the compression of the bilayer of N-Py-500 and AuNPs, leading to a decrease in the adsorption rate. This problem of Fe ion dissolution was effectively solved by adding excess $Ca(OH)_2$ to the system of adsorption experiments.

In addition, the reproducibility of N-Py-500 and the desorption of gold nanoparticles were studied. After four adsorption–desorption experiments with 10% thiourea and 2% hydrochloric acid mixed reagent as the desorbent, the adsorption efficiency of N-Py-500 was still up to 92.1%, and the desorption efficiency of gold nanoparticles was up to 94.2%. Therefore, N-Py-500 can be reused as an adsorbent, and the adsorbed gold nanoparticles can also be desorbed for reuse.

Combined with FTIR and XPS analyses, it was found that there might be some chemical reactions between N-Py-500 and AuNPs in addition to electrostatic interactions.

Generally, it found that oxidised pyrite, thermally modified at 500°C, exhibited efficient adsorption of gold nanoparticles across a wide pH range (2-7) and that the gold nanoparticles could be desorbed and recovered under specific conditions. Therefore, thermally modified pyrite is expected to serve as a cost-effective and efficient gold nanoparticle adsorbent for larger-scale applications. In conclusion, thermally modified pyrite is a promising and reusable efficient adsorbent for AuNPs. For further applications, the adsorption of thermally modified pyrite on AuNPs under more complex environmental media conditions, for example with other inorganic or organic pollutants, are areas for future research.

Conflicts of interest

There are no conflicts to declare.

Data availability

All data will be made available by the authors upon reasonable request.

Acknowledgements

This work was financially supported by the National Natural Science Foundation of China (42162006, 42163010), Guizhou Provincial Basic Research Program (Natural Science) (QKHJC [2020] 1Y171) and Guizhou Normal University Academic Seedling Fund (Qianshi Xinmiao [2022] No. 24).

References

Amstaetter, K., Borch, T., & Larese-Casanova, P. (2010). Redox transformation of arsenic by Fe (II)-Activated Goethite (α -FeOOH). Environmental Science and Technology, 44(1), 102 – 108.

Arturo, Keller, A., & Lazareva. (2014). Predicted releases of engineered nanomaterials: From global to regional to local. Environmental Science and Technology Letters.

Banfield, J. F., & Zhang, H. Z. (2001). Nanoparticles in the environment. Reviews in Mineralogy and Geochemistry, 44(1), 1 – 58. https://doi. org/10. 2138/rmg. 2001. 44. 01.

Dedeh, A., Ciutat, A., Treguer-Delapierre, M., & Bourdineaud, J. -P. (2015). Impact of gold nanoparticles on zebrafish exposed to a spiked sediment. Nanotoxicology, 9(1), 71 – 80. https://doi. org/10. 3109/17435390. 2014. 889238.

Dong, Y., Liu, Z., Liu, W., & Lin, H. (2022). A new organosilane passivation agent prepared at ambient temperatures to inhibit pyrite oxidation for acid mine drainage control. Journal of Environmental Management, 320, 115835. https://doi. org/10. 1016/j. jenvman. 2022. 115835.

Fan, R., Xie, F., Guan, X., Zhang, Q., & Luo, Z. (2014). Selective adsorption and recovery of Au(III) from three kinds of acidic systems by persimmon residual based bio-sorbent: A method for gold recycling from e-wastes. Bioresource Technology, 163, 167 – 171. https://doi. org/10. 1016/j. biortech. 2014. 03. 164.

Frens, G. (1973). Controlled nucleation for the regulation of the particle size in monodisperse gold suspensions. Nature Physical Science, 241(105), 20 – 22. https://doi. org/10. 1038/physci241020a0.

Fu, Y. H., Wu, C., Liu, Q., Li, S. S., Li, S., Zhang, S., Wan, Q. (2024). Highly efficient recovery of gold by thermally modified pyrite and its mechanism. Minerals Engineering 219 (2024) 109075. https://doi.org/10.1016/j.mineng. 2024. 109075.

Guo, Y., Li, C., Gong, Z., Guo, Y., Wang, X., Gao, B., Qin, W., & Wang, G. (2020). Photocatalytic decontamination of tetracycline and Cr(VI) by a novel α -FeOOH/FeS2 photocatalyst: One-pot hydrothermal synthesis and Z-scheme reaction mechanism insight. Journal of Hazardous Materials, 397, 122580. https://doi. org/10. 1016/j. jhazmat. 2020. 122580.

He, X., Min, X., Peng, T., Ke, Y., Zhao, F., Wang, Y., & Sillanpää, M. (2019). Highly efficient antimonate removal from water by pyrite/hematite bi-mineral: Performance and mechanism studies. Journal of Chemical and Engineering Data, 64(12), 5910 – 5919. https://doi. org/10. 1021/acs. jced. 9b00801.

Hochella, M. F. (2002). Nanoscience and technology the next revolution in the earth sciences. Earth and Planetary Science Letters, 203(2), 593 – 605. https://doi. org/10. 1016/S0012-821X(02)00818-X.

Hochella, M. F., Jr., Lower, S. K., Maurice, P. A., Penn, R. L., Sahai, N., Sparks, D. L., & Twining, B. S. (2008). Nanominerals, mineral nanoparticles, and Earth systems. Science, 319(5870), 1631 – 1635. https://doi. org/10. 1126/science. 1141134.

Isoda, K., Tanaka, A., & Fuzimori, C. (2020). Toxicity of gold nanoparticles in mice due to nanoparticle/drug interaction induces acute kidney damage. Nanoscale Research Letters, 15, 1 – 8.

Jiang, W. R., Tu, Z. H., & Zhou, S. (2021). Progress in the study of surface oxidation mechanism and kinetic influencing factors of pyrite. Metal Mining, 03, 88 – 102.

Kalaitzidou, K., & Merachtsaki, D. (2023). Post-use recovery of nanoparticles. In K. Simeonidis & S. Mourdikoudis (Eds.), Nanoparticles as sustainable environmental remediation agents, 61 p. 0. Royal Society of Chemistry.

Kaur, G., Singh, B., Singh, P., Kaur, M., Buttar, K. K., Singh, K., Thakur, A., Bala, R., Kumar, M., & Kumar, A. (2016). Preferentially grown nanostructured iron disulfide (FeS2) for removal of industrial pollutants. RSC Advances, 6(101), 99120 – 99128. https://doi. org/10. 1039/C6RA18838A.

Keller, A. A., McFerran, S., Lazareva, A., & Suh, S. (2013). Global life cycle releases of engineered nanomaterials. Journal of Nanoparticle Research, 15(6). https://doi. org/10. 1007/s11051-013-1692-4.

Kenzhaliyev, B., Surkova, T., Yessimova, D., Baltabekova, Z., Abikak, Y., Abdikerim, B., & Dosymbayeva, Z. (2023). Extraction of noble metals from pyrite cinders. ChemEngineering, 7(1), 14. https://doi. org/10. 3390/chemengineering7010014.

Krishnamurthy, S., & Yun, Y. -S. (2013). Recovery of microbially synthesised gold nanoparticles using sodium citrate and detergents. Chemical Engineering Journal, 214, 253 – 261. https://doi. org/10. 1016/j. cej. 2012. 10. 028.

Lazim, A. M., Eastoe, J., Bradley, M., Trickett, K., Mohamed, A., & Rogers, S. E. (2010). Recovery

of gold nanoparticles using pH-sensitive microgels. Soft Matter, 6(9), 2050 – 2055. https://doi. org/10. 1039/c002511a.

Lee, J., Mahendra, S., & Alvarez, P. J. J. (2010). Nanomaterials in the construction industry: A review of their applications and environmental health and safety considerations. ACS Nano, 4(7), 3580 – 3590. https://doi. org/10. 1021/nn100866w.

Li, P. (2016). Structural and physical evolution of heat-treated pyrite and its chemical reactivity [Unpublished PhD thesis]. Hefei University of Technology.

Lu, L., Wang, R., & Xue, J. (2005). Prosperity; Chen, Jun, Experimental study on the oxidation rate of pyrite. Science in china (series D: earth sciences), 05, 434 – 440.

Luo, S., Nie, X., Yang, M., Fu, Y. H., Zeng, P., & Wan, Q. (2018). Sorption of differently charged gold nanoparticles on synthetic pyrite. Minerals, 8(10), 428. https://doi. org/10. 3390/min8100428.

Luty-Błocho, M., Wojnicki, M., Tokarski, T., Hessel, V., & Fitzner, K. (2021). Batch Reactor vs. microreactor System for Efficient AuNP Deposition on Activated Carbon Fibers. Materials, 14(21), 6598. https://doi. org/10. 3390/ma14216598.

Mikhlin, Y., Likhatski, M., Karacharov, A., Zaikovski, V., & Krylov, A. (2009). Formation of gold and gold sulfide nanoparticles and mesoscale intermediate structures in the reactions of aqueous HAuCl4 with sulfide and citrate ions. Physical Chemistry Chemical Physics, 11(26), 5445 – 5454. https://doi. org/10. 1039/b823539b.

Murphy, R., & Strongin, D. R. (2009). Surface reactivity of pyrite and related sulfides. Surface Science Reports, 64(1), 1 – 45. https://doi. org/10. 1016/j. surfrep. 2008. 09. 002.

Novikov, A. P., Kalmykov, S. N., Utsunomiya, S., Ewing, R. C., Horreard, F., Merkulov, A., Clark, S. B., Tkachev, V. V., & Myasoedov, B. F. (2006). Colloid transport of plutonium in the far-field of the Mayak Production Association, Russia. Science, 314(5799), 638 – 641. https://doi. org/10. 1126/science. 1131307.

Pan, Y., Neuss, S., Leifert, A., Fischler, M., Wen, F., Simon, U., Schmid, G., Brandau, W., & Jahnen-Dechent, W. (2007). Size-dependent cytotoxicity of gold nanoparticles. Small, 3(11), 1941 – 1949. https://doi. org/10. 1002/smll. 200700378.

Park, J. -W., & Shumaker-Parry, J. S. (2014). Structural study of citrate layers on gold nanoparticles: Role of intermolecular interactions in stabilizing nanoparticles. Journal of the American Chemical Society, 136(5), 1907 – 1921. https://doi. org/10. 1021/ja4097384.

Pernodet, N., Fang, X. H., Sun, Y., Bakhtina, A., Ramakrishnan, A., Sokolov, J., Ulman, A., & Rafailovich, M. (2006). Adverse effects of citrate/gold nanoparticles on human dermal fibroblasts. Small, 2(6), 766 – 773. https://doi. org/10. 1002/smll. 200500492.

Rashid, J., Saleem, S., Awan, S. U., Iqbal, A., Kumar, R., Barakat, M. A., Arshad, M., Zaheer, M., Rafique, M., & Awad, M. (2018). Stabilized fabrication of anatase-TiO 2/FeS 2 (pyrite) semiconductor composite nanocrystals for enhanced solar light-mediated photocatalytic degradation of methylene blue. RSC Advances, 8(22), 11935 – 11945. https://doi. org/10. 1039/c8ra02077a.

Rex M, C., Anand, S., Rai, P. K., & Mukherjee, A. (2023). Engineered nanoparticles (ENPs) in the aquatic environment: An overview of their fate and transformations. Water, Air, and Soil Pollution, 234(7). https://doi. org/10. 1007/s11270-023-06488-1.

Wang, Y., Fu, Y. H., & Liu, Q. (2023). Adsorption behavior of iron (hydrogen) oxide on gold nanoparticles. Journal of Guizhou Normal University (Natural Science Edition), 41(05), 68 – 77.

Waters, K. E., Rowson, N. A., Greenwood, R. W., & Williams, A. J. (2008). The effect of heat treatment on the magnetic properties of pyrite. Minerals Engineering, 21(9), 679 – 682. https://doi.

org/10. 1016/j. mineng. 2008. 01. 008.

Wiwanitkit, V., Sereemaspun, A., & Rojanathanes, R. (2009). Effect of gold nanoparticles on spermatozoa: The first world report. Fertility and Sterility, 91(1), e7–e8. https://doi. org/10. 1016/j. fertnstert. 2007. 08. 021.

Yang, M., Wan, Q., Nie, X., Luo, S., Fu, Y. H., Zeng, P., & Luo, W. (2021). Quantitative XPS characterization of "invisible gold" in Carlin-type gold ores through controlled acid erosion. Journal of Analytical Atomic Spectrometry, 36(9), 1900–1911. https://doi. org/10. 1039/D1JA00102G.

Yang, X., Mu, Y., & Peng, Y. (2021). Comparing lead and copper activation on pyrite with different degrees of surface oxidation. Minerals Engineering, 168, 106926. https://doi. org/10. 1016/j. mineng. 2021. 106926.